10th International Conference on Fracture Mechanics of Concrete and Concrete Structures
FraMCoS-X
G. Pijaudier-Cabot, P. Grassl and C. La Borderie (Eds)
https://doi.org/10.21012/FC10.235473

# MESOSCALE ANALYSIS FOR THE BOND BEHAVIOR OF CONCRETE UNDER ACTIVE CONFINEMENT USING COUPLED RBSM AND SOLID FEM

MUHAMMAD SHOAIB KARAM*, YOSHIHITO YAMAMOTO†, HIKARU NAKAMURA †† AND TAITO MIURA†††

Nagoya University
Nagoya, Japan
*shoaib.karam@gmail.com
† y.yamamoto@civil.nagoya-u.ac.jp
†† hikaru@cc.nagoya-u.ac.jp
††† t.miura@civil.nagoya-u.ac.jp

**Key words:** Bond Characteristics, Pull-out Test, Active Confinement, Coupled RBSM and Solid FEM, Friction Sensitivity Analysis

**Abstract:** The research manuscript deals with the brief introduction to the development and the validation of the new coupled numerical formulation, comprised of the Rigid Body Spring Model (RBSM) and the solid Finite Element Method (FEM) evaluating the bond behavior and failure mechanism of the actively confined and unconfined RC specimens loaded under pull-out test. The RBSM has been referred as an effective numerical framework for the evaluation of nonlinear mechanical response of concrete, quantitatively. However, the modeling of the reinforcing steel in RBSM has difficulty for simulating the complex behavior of steel such as elastoplasticity. Therefore, this limitation refers towards the development of new numerical formulation, i.e., coupled RBSM-FEM. In coupled RBSM-FEM, steel embedded in concrete is modeled using eight noded nonlinear solid finite elements considering the actual geometrical features e.g., rib height, shape and lug spacing, etc. In the coupled numerical formulation, concrete is modeled using RBSM. The boundary interfaces between concrete and steel (Solid FEM) has been accomplished through link element. The link element on the interface between RBSM element and solid FEM element consists of two shear springs and one normal spring. The proposed model is validated through the experimental investigations on RC specimens loaded under pull-out test with and without externally applied normal pressure. The proposed model has capability to simulate the internal fracture mechanism of concrete and elastoplastic behavior of the steel.

## 1 INTRODUCTION

The bond between steel and concrete is an important parameter that influences the overall structural performance when the system is loaded. There is a wide range of variables that alter the effectiveness of the bond strength properties between steel and concrete, e.g., concrete type and its mechanical properties, embedment length, diameter of the steel reinforcement, geometrical features of steel (rib height, shape and lug spacing, etc.), concrete cover thickness and amount of confinement (active and passive) applied, etc. [1-4]. The bond resistance mechanism of steel and concrete has been investigated experimentally by many researchers under various boundary conditions. It was investigated that the bond strength was highly dependent on the degree of confinement (passive confinement, i.e. through the concrete cover thickness and transverse reinforcement and active confinement, i.e. through external pressure). The mode of failures (splitting and pull-out, etc.) were also influenced by the amount of confinement applied. The studies revealed that the bond strength and ultimate slip for deformed rebars increased as the active confinement increased while other parameters were kept constant. The confinement provided by the concrete cover and lateral reinforcing bars affected the bond splitting stress and cracking for reinforced concrete plates under uniaxial and biaxial tension [5]. Similarly, the stress distribution variation inside the concrete and uneven contact pressure and friction between the concrete block and steel plate interface also affected the bond strength of the reinforced concrete block in pull-out test [6].

On the other hand, in recent years, attempts have been made to evaluate the complex variations in bond characteristics under various conditions by mesoscale model simulations. Researchers like Hayashi et al. [7], Nagai et al. [8], Matsumoto et al. [9], Eddy et al. [10-11], used three dimensional Rigid-Body-Spring Model (3D RBSM) with a mesoscale model directly expressed from the rib shape and size of deformed rebar, had succeeded in reproducing crack propagation behaviors and their performances of RC members and structures. Their models were effective to express the complex bond characteristics. However, in their models, reinforcing bars were modeled by RBSM using a regular mesh. RBSM is a kind of discrete type model proposed by Kawai [12]. It is well known that cracking behavior and failure localization behavior can be reproduced by using random polyhedral mesh using Voronoi diagram. On the other hand, it is also confirmed that the Poisson's effect cannot be reproduced when a regular mesh is used. Therefore, the existing mesoscale models using RBSM have limitation in reproducing the elastic behavior of the reinforcing bar. Furthermore, the Poisson's effect although can be captured by using RBSM with a random polyhedron. However, in that case, it is difficult to simulate the macroscopic elasto-plastic response of the reinforcing bar.

In this study, the coupled RBSM and solid FEM model as shown in Fig. 1 is proposed to overcome the limitations of the existing mesoscale models using RBSM. In the proposed model, reinforcing steel bars embedded in concrete are modeled using eight-noded nonlinear solid finite elements considering the actual geometrical details, e.g., rib height, shape and lug spacing, etc. To validate the model, pull-out tests of reinforced concrete specimens under lateral pressure are simulated. The focus is especially made on the effects of stress conditions and boundary conditions on bond characteristics, crack propagation behaviors and failure modes.

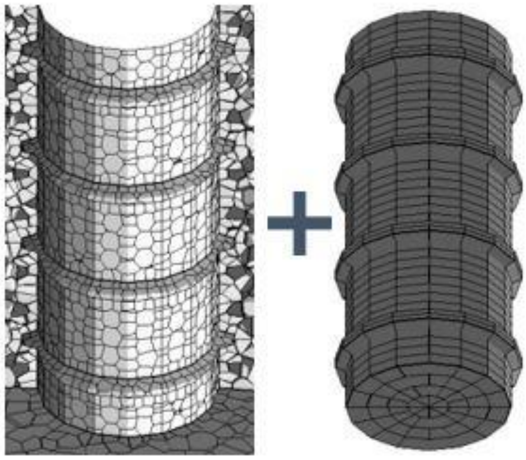


**Figure 1:** Coupled RBSM and Solid FEM.

## 2 NUMERICAL MODELS

### 2.1 Concrete model

Concrete is modeled using 3D-RBSM. The 3D-RBSM has been referred as an effective numerical framework for the evaluation of nonlinear mechanical response of concrete quantitatively such as crack propagation, shear transfer behavior of cracked surfaces, and compression failure behaviors including localization and constraint pressure dependence [13]. Cracks initiate and propagate through the interface boundaries and thus are strongly affected by the mesh design. To address this, random geometry of rigid particles is generated using Voronoi diagram as shown in Fig. 2.

The response of the spring model provides an insight into the interaction among the

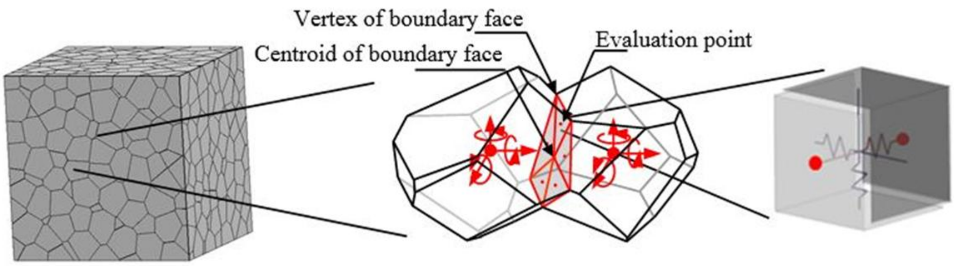


**Figure 2:** 3D-RBSM and Voronoi diagram**.**

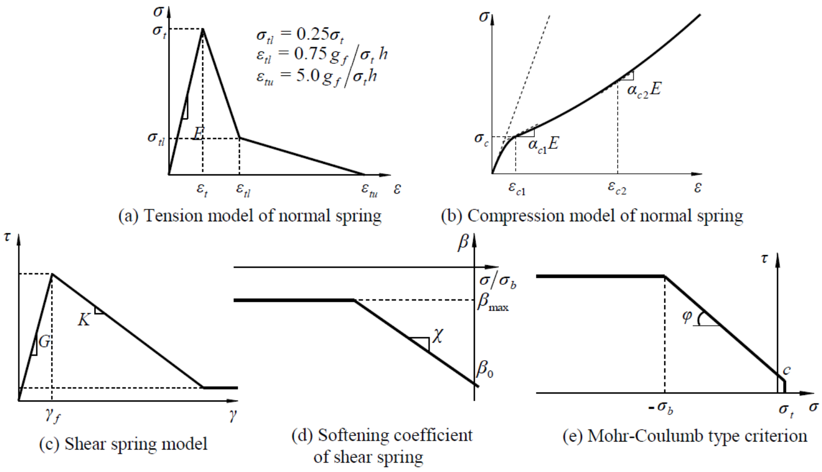


**Figure 3:** Constitutive model for concrete (Yamamoto et al., 2008).

**Table 1:** Calibrated model parameters of normal spring

| Elastic Modulus | Tensile Response | | Compressive Response | | | |
|---|---|---|---|---|---|---|
| $E$ (N/mm$^2$) | $\sigma_t$ (N/mm$^2$) | $g_f$ (N/mm) | $\sigma_c$ (N/mm$^2$) | $\varepsilon_{c2}$ | $\alpha_{c1}$ | $\alpha_{c2}$ |
| $1.4E^*$ | $0.65f_t^*$ | $0.5G_F^*$ | $1.5f_c'^*$ | -0.015 | 0.15 | 0.25 |

**Table 2:** Calibrated model parameters of shear spring

| Elastic Modulus | Fracture Criterion | | | Softening Behavior | | | |
|---|---|---|---|---|---|---|---|
| $G$ (N/mm$^2$) | $c$ (N/mm$^2$) | $\varphi$ (degree) | $\sigma_b$ (N/mm$^2$) | $\beta_0$ | $\beta_{max}$ | $\chi$ | $\kappa$ |
| $0.35E$ | $0.14 f_c'^*$ | 37 | $1.00f_c'^*$ | -0.05 | -0.025 | -0.01 | -0.3 |

** The macroscopic material parameters obtained from the concrete specimen's test*
*$E^*$: Young's Modulus, $f_t^*$: Tensile Strength, $G_F^*$: Fracture Energy, $f_c'^*$: Compressive Strength*

particles. In this model, each rigid particle has three translational and three rotational degrees of freedom defined at the nuclei (or nodal points) that define the particles according to the Voronoi diagram. The boundary surface of two particles is divided into several triangles with a center of gravity and vertices of the surface as shown in the Fig. 2. One normal and two shear springs are set at the center of each triangle. The distribution of springs in this way, over the Voronoi facet common to two neighboring nodal points, this model also

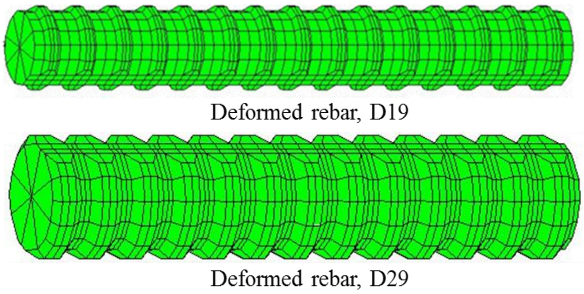


**Figure 4:** 3D model of steel reinforcement.

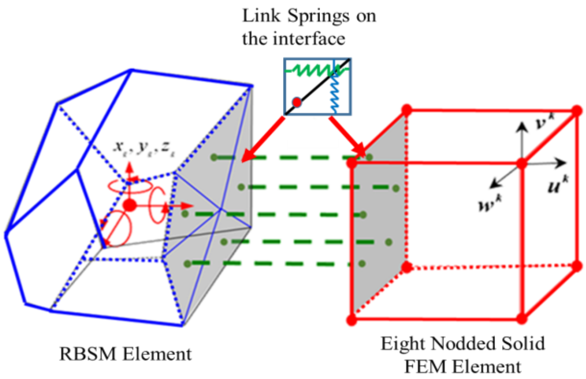


**Figure 5:** RBSM and solid FEM boundary interface.

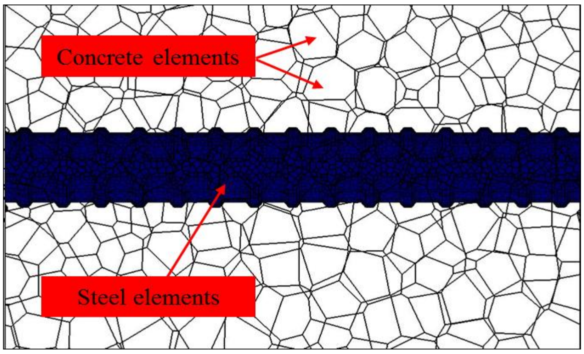


**Figure 6:** Representation of the elements.

accounts for the effects of bending and torsional moment without the need to set any rotational springs [14]. Models that can reproduce the softening and localization behavior under various stresses, proposed by Yamamoto et al. are applied to the constitutive model of the spring as shown in Fig. 3.

The material parameters of the constitutive models have been calibrated by conducting parametric analyses comparing with the test results of uniaxial tension, uniaxial compression, hydrostatic compression and triaxial compression. The calibrated parameters for normal and shear springs are shown in Table 1 and Table 2, respectively. It has been confirmed that the proposed model can reasonably simulate the propagation of visible crack and especially the localization length of compression fracture in concrete in the case of that the average mesh size is from 10 mm to 30 mm.

## 2.2 Model of reinforcing bar

The reinforcing steel bar embedded in concrete is modeled using eight noded nonlinear solid FEM considering the actual geometrical features e.g., rib height, shape and lug spacing, etc. account for the proper interlocking with the surrounding concrete. The model has been shown in Fig. 4. A Von Mises plasticity model with strain hardening is used for the constitutive model.

## 2.3 Concrete-Steel interface

The boundary interfaces between concrete (3D-RBSM) and steel (Solid FEM) have been accomplished through link element. The link element on the interface between concrete (3D-RBSM) element and steel (Solid FEM) element consists of two shear springs and one normal spring as shown in Fig. 5. The constitutive model of normal and shear springs on boundary interface are same with concrete model (shown in Fig. 3). However, the tensile strength of the normal spring on the boundary interface has been reduced to half. The proposed coupled RBSM-FEM formulation has capability to generate the link elements arbitrarily on the boundary interface thus reduces the computational cost. The deformation of each spring of link element is obtained by the relative displacement between the surfaces of both elements. The average mesh size near to the boundary interface of concrete element (3D-RBSM) and steel element (solid FEM) is selected less than the rib height of the steel reinforcement for the proper representation of the geometrical features of the steel reinforcment as shown in Fig. 6. The selected average mesh size in present mesoscale simulations ranges between around 1.5 mm to 10 mm.

## 3 SIMULATION OF UNCONFINED AND CONFINED SPECIMENS

### 3.1 Test overview and numerical modelling

In this manuscript, the numerical simulations are carried out for the already published test results on RC specimens loaded under pull-out test with and without application of the normal perrssure [15]. All the specimens were cube with the size of 150 x 150 x 150 $mm^3$. The specimens were embedded with deformed bars of D19 and D29. The yield strength ($f_y$) of the steel reinforcement was approximately 632.30 MPa. The concrete compressive strength of the specimens was approximately 32.5 MPa. The embedment length of reinforcing bar was 150 mm for all the specimens. The specimens were seated on a system of bearing plates and a spherically bearing block to insure the load would be purely axial. A leather pad of around 1.5 mm thickness was placed between the concrete specimens and the bearing steel plates. The normal pressure was applied to two parallel concrete faces of 150 mm cube specimens using a loading frame which enclosed the test specimens, hydraulic ram and spherically seated bearing blocks. A dial micrometer gage was used to determine the movement of the deformed bar to the concrete.

The numerical simulations are mainly divided into three cases. The specimens embedded with deformed rebar D19, without and with application of the normal pressure are termed as case 1 and case 2, respectively. Similarly, the unconfined specimens embedded with deformed rebar D29, is considered as case 3. Initially, the numerical validation of the case 1 and case 2 was performed, the numerical simulations were further extended for case 3 after numerical validations of case 1 and case 2. The numerical models corresponding to all three cases have been illustrated in Fig. 7. The average mesh size in all the cases around the

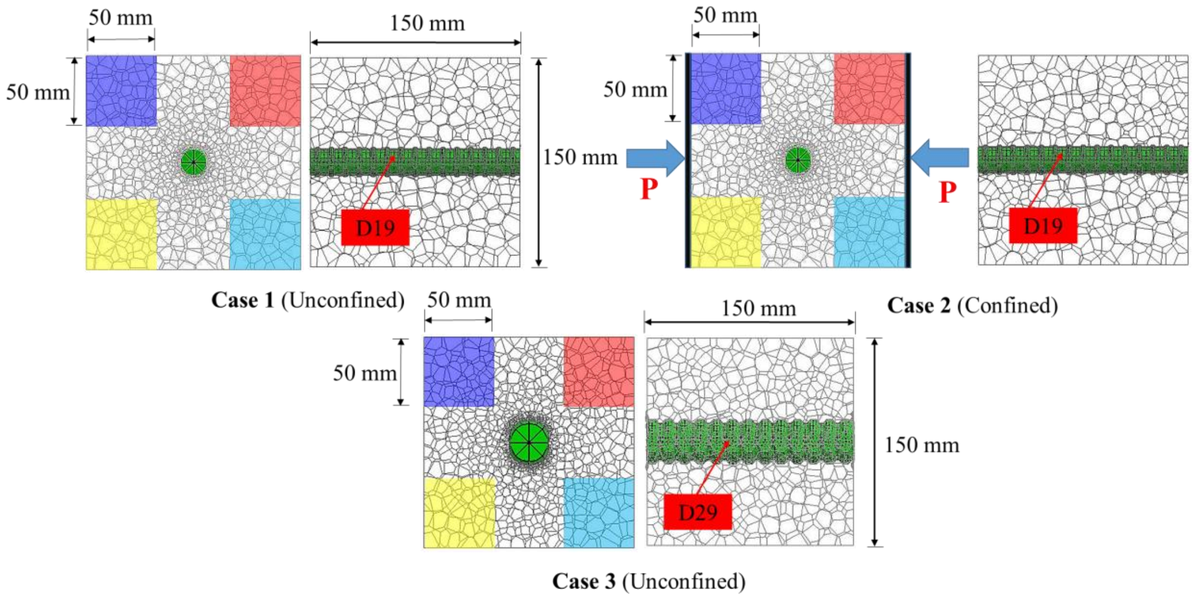


**Figure 7:** Numerical models.

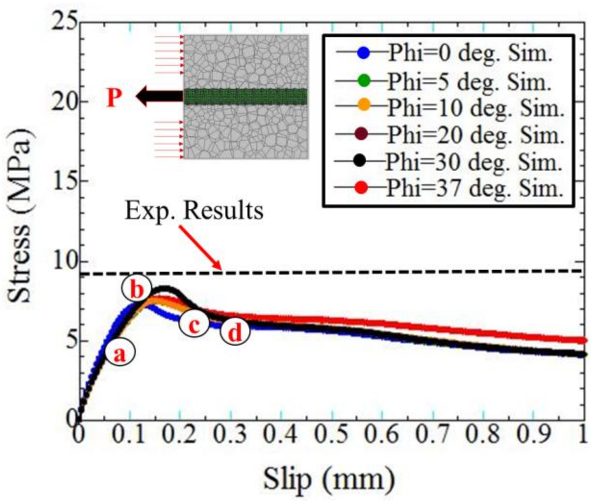


**Figure 8:** Stress slip relations of case 1.

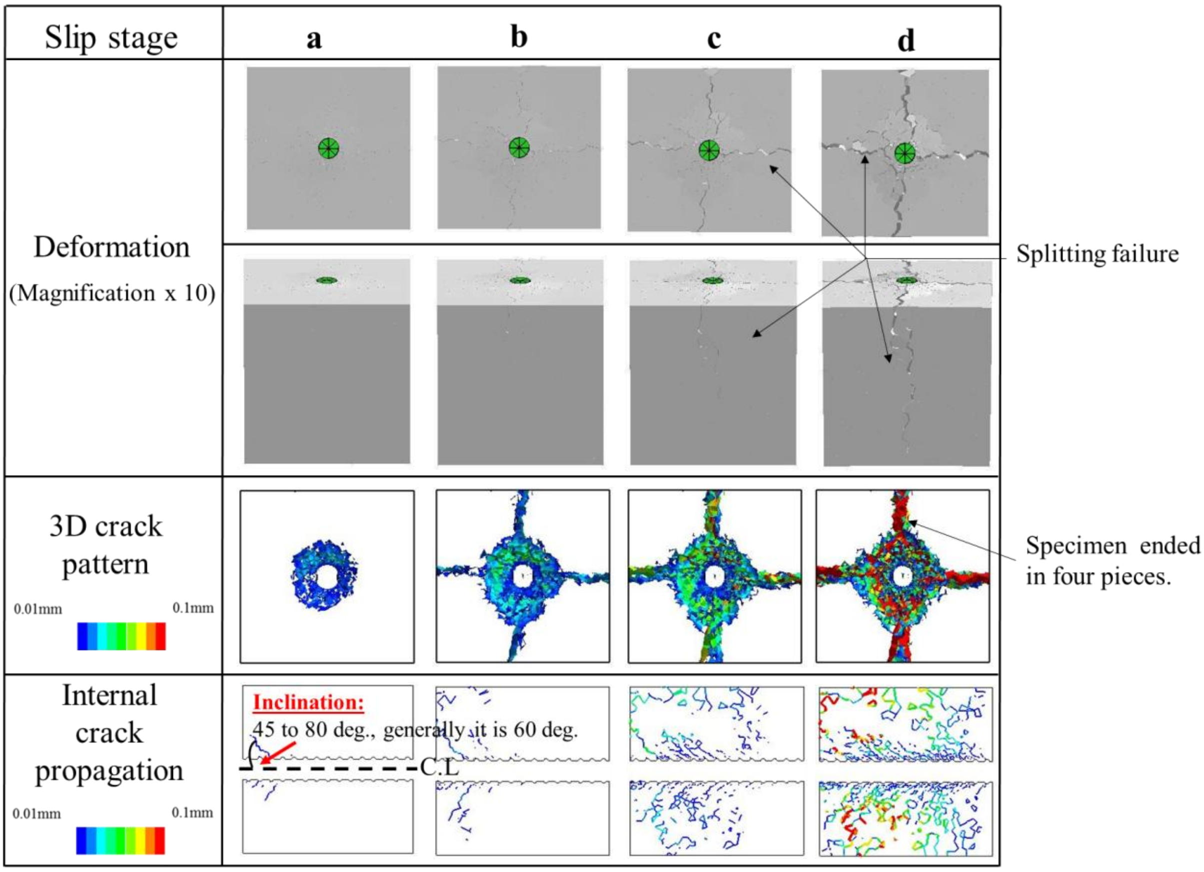


**Figure 9:** Deformed behaviors of case 1.

rebar is 1.5 mm. The relatively large mesh size is selected at the ends to reduce the computational cost.

The preliminary numerical investigation suggests that the pull off region of concrete cones may be influenced by the reaction force generated against the different size of plates, thus affects the overall deformed behaviors and bond strength. The limited details for the boundaries in the test necessitate to select the reasonable numbers and size of the loading plates in the numerical simulations which should not affect the pull off region of concrete cone under the pull-out test. Therefore, the four number of plates are used in numerical modelling to address the above-mentioned facts. The size of each plate is 50 x 50 mm$^2$ as shown in Fig. 7.

## 4 RESULTS AND DISCUSSION

### 4.1 Case 1 (Unconfined specimen embedded with rebar D19)

As discussed earlier, the boundary conditions for the plates in the experiment play a significant role in controlling the deformation capacity and deformed behaviors. Therefore, it is important to consider the boundary conditions of test adequately, for high precision numerical simulations. The leather pad between the concrete specimens and the bearing steel plates (section 3.1) may influence the level of friction and thus reaction force imparted on concrete surface and ultimately may alter the bond strength. To address this test arrangement in simulations, different friction levels are investigated numerically between the concrete specimens and the steel plates through the sensitivity analaysis of friction. The friction between the steel plates and concrete elements is controlled by the parameters of Mohr-Coulomb criteria of shear spring between the elements (Figure 3e), where c and $\varphi$ are cohesion and the angle of internal friction, respectively. In sensitivity analysis of friction, the different levels of friction between the concrete specimens and the steel plates are incorporated by selecting the different angles of internal friction ($\varphi$) for shear springs to lie between 0 and 37 degrees. The numerical simulation results for case 1 considering the sensitivity analysis of friction has been illustrated in Fig. 8.

It is evident from the Fig. 8, the stress slip relationships are dependent on the friction between the concrete specimen and the bearing steel plates. The Fig. 8 shows that for low friction ($\varphi = 0, 5,$ and 10 deg.) levels, the simulations results are on the lower side compared with the other friction levels ($\varphi = 20, 30$ and 37 deg.). The cases corresponding to internal friction angle equal to 20 deg. and 30 deg. show almost the same behavior, and express the maximum bond stress close to the test value. On the other hand, the case where the internal friction angle is 37 deg., the maximum bond stress decreases a little.

Fig. 9 shows deformation behaviors obtained by simulation, corresponding to case with the internal friction angle of 20 degrees. At point a on stress slip curve, it can be confirmed that the cracks propagate conically from the surface of the reinforcing bar, as investigated by Goto [16]. Furthermore, at point b, splitting cracks occur. At point d, it can be seen that the cracks propagate to the ends of the specimen. The simulation failure mode is consistent with the experimental results.

### 4.2 Case 2 (Confined specimen embedded with rebar D19)

The numerical simulation results of specimen confined by normal pressure (50% of $f_c'$) are discussed here. The numerical simulation of case 2 is also based on the sensitivity analysis of friction between the concrete specimens and the bearing steel plates while externally applied normal pressure is kept constant. The simulation results of case 2 are shown in Fig. 10. The Fig. 10 shows that the applied normal pressure increases the ultimate bond stress and ultimate slip compared with unconfined specimen (case 1). The stress slip relationships show that the numerical results are also highly sensitive to

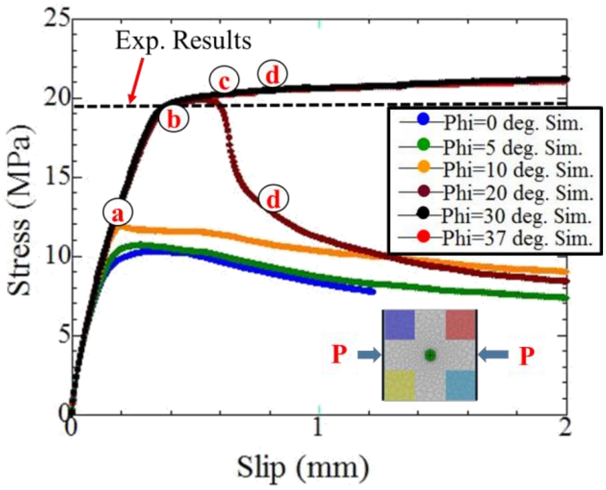


**Figure 10:** Stress slip relations of case 2.

the friction between concrete and steel bearing plates. The Fig. 10 shows that for low friction ($\varphi = 0, 5,$ and 10 deg.) levels, the simulations results are on the lower side. It is evident from stress slip curve, in the case where the internal friction angle is 20 deg., the simulated stress slip results are found in agreement to experimental results and also express softening behavior. On the other hand, when the internal friction angle is 30 deg. or more, the rebar yields and no softening appears.

The numerical investigations can be clarified through the deformed behaviors. The deformed behaviors only for mild friction level ($\varphi = 20$ deg.) and high friction level ($\varphi = 30$ deg.) are shown in Fig. 11 and Fig. 12, respectively. In very low friction levels ($\varphi$=0, 5, and 10 deg.), specimen shows the splitting type failure, although not shown here. In mild friction level ($\varphi = 20$ deg.) the specimen produces the mixed type failure, i.e., the splitting as well as the pull-out (Fig. 11). In confined specimen with mild friction level, crack propagation is observed from one pressure face to other pressure face and then extends longitudinally investigated experimentally and numerically. Furthermore, that crack also intersects the embedded rebar as shown in Fig. 11. On the other hand, high friction level the stress slip relations and deformed behaviors changed as confirmed through Fig. 10 and Fig. 12 respectively. In high friction level ($\varphi > 20$ deg.), no

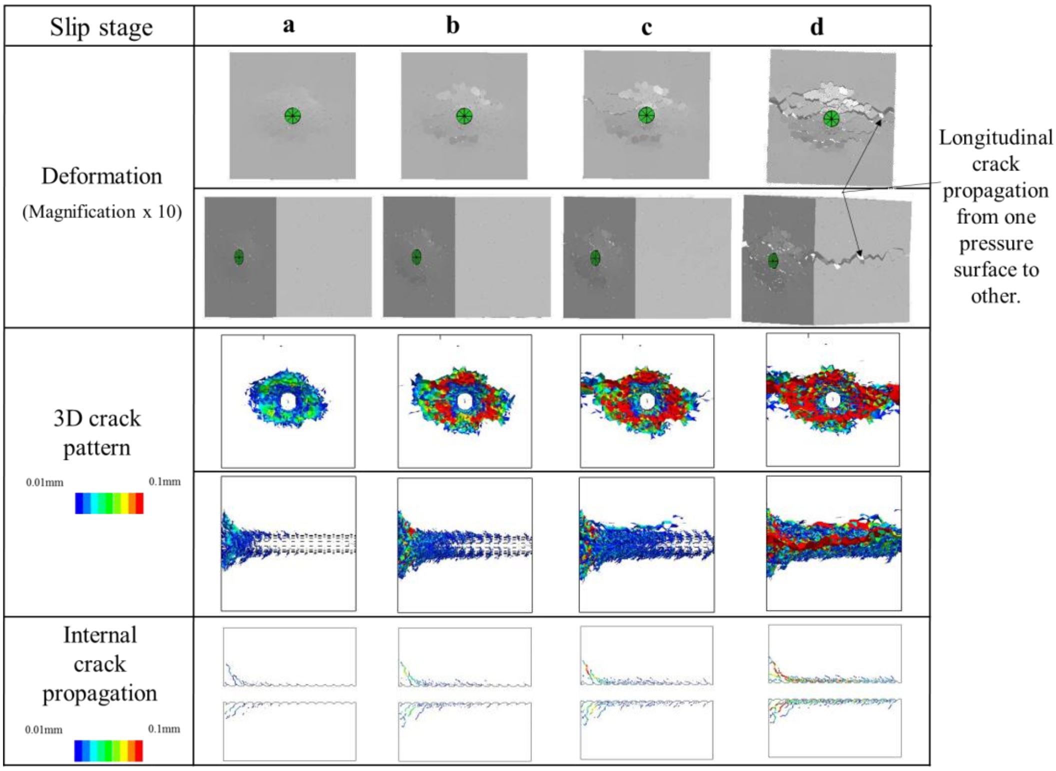


**Figure 11:** Deformed behaviors of case 2 ($\varphi = 20$ deg.).

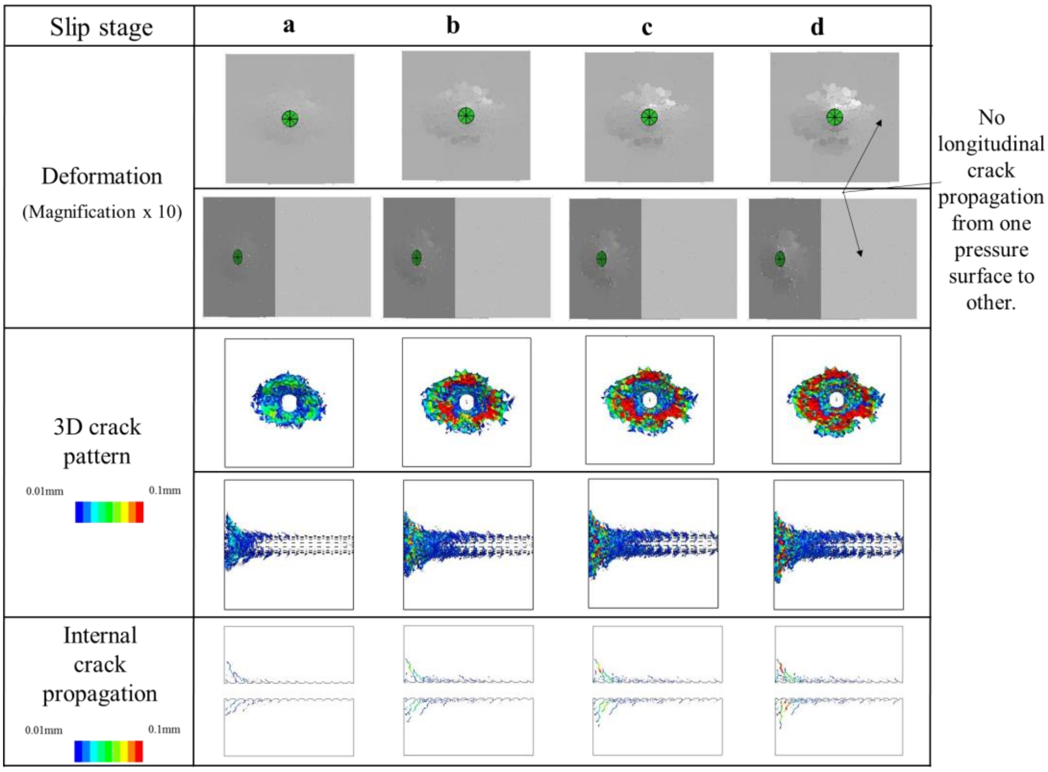


**Figure 12:** Deformed behaviors of case 2 ($\varphi = 30$ deg.).

longitudinal crack propagation is observed from one pressure face to other pressure face compared with mild friction level.

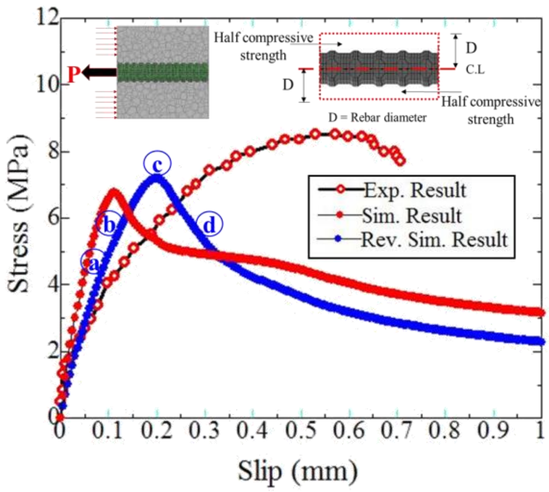


**Figure 13:** Stress slip relations of case 3.

cement ratio and the aggregates did not come close to the rebar because of the wall effect [17]. These interfacial transition zones around the rebar should be simulated with reduced concrete compressive strength. The concrete compressive should be reduced to half around the rebar and the influence area ranged equal to one diameter (1D) of rebar from its center [1]. The original model has been revised based on the recommendation of previous researchers. The Fig. 13 shows that the revised model effectively captures the ultimate stress but slightly under estimates the experimental peak slip. The deformed behaviors of case 3 have been shown in Fig. 14. The specimen in

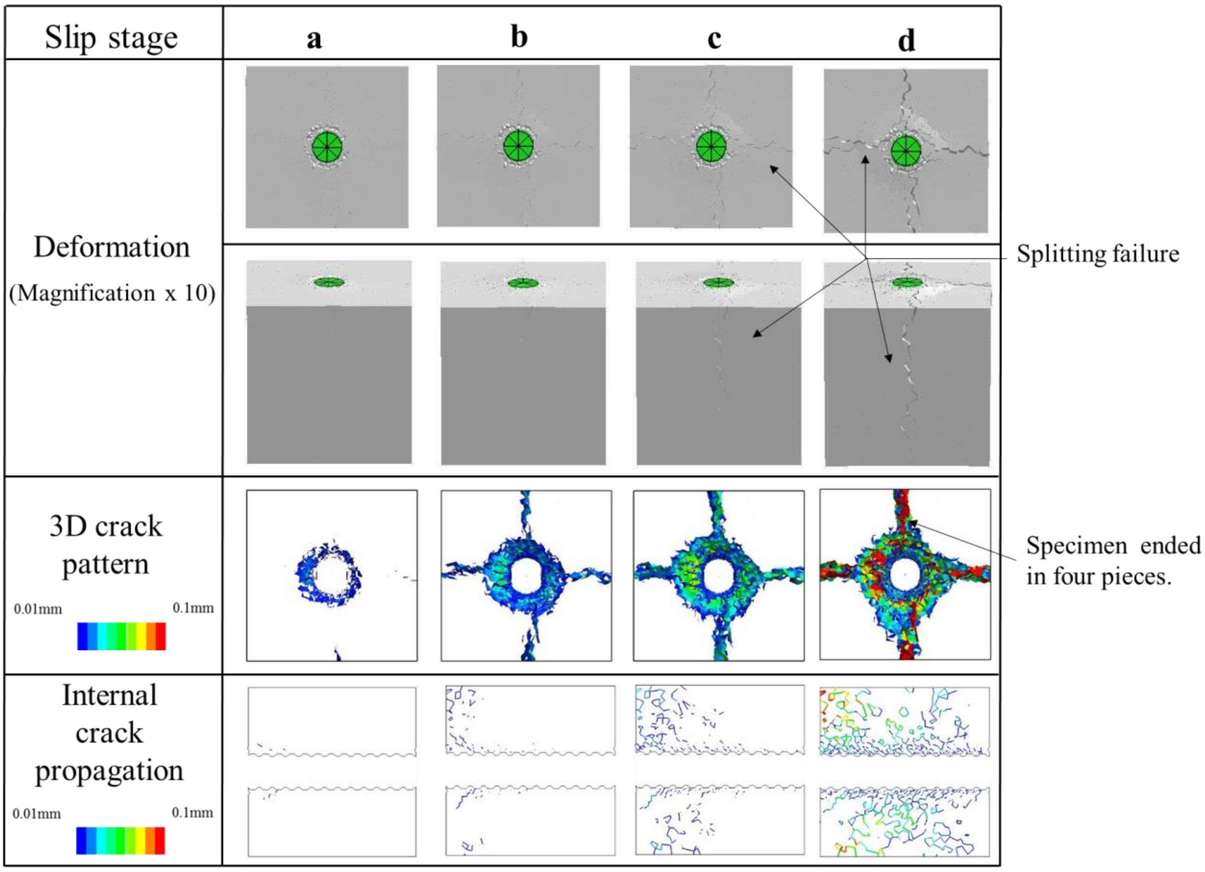


**Figure 14:** Deformed behaviors of case 3.

### 4.3 Case 3 (Unconfined specimen embedded with rebar D29)

The numerical validation of case 3 only based on the mild friction ($\varphi = 20$ deg.) level. The simulation results are shown in Fig. 13. The previous investigations revealed that the regions around the rebar had high water case 3 also shows the radial crack development from reinforcing bar same as of case 1 and the specimen ends into four pieces, causes splitting type failure.

## 5 CONCLUSIONS

The numerical simulations are conducted through proposed coupled numerical formulation, comprised of the Rigid Body Spring Model (RBSM) and the solid Finite Element Method (FEM) evaluating numerically the bond behavior and fracture mechanism of the actively confined and unconfined RC specimens. Based on the mesoscale numerical analysis, the following conclusions can be drawn.

1) The unconfined RC specimens (case 1 and case 3) express lower bond strength compared with actively confined specimens (case 2), experimentally and numerically. Whereas, the confined specimens show increased bond strength and slip at ultimate. The slip at ultimate bond stress increased with increased normal pressure. It is also confirmed through simulation results that the confinement effect of normal pressure is considered appropriately in numerical analysis.
2) The internal fracture mechanism is also revealed by the simulation results, the unconfined concrete specimens (case 1 and case 3) show longitudinal radial crack development from reinforcing bar, causing splitting type failure. Whereas, the confined concrete specimens demonstrate relatively improved performance and display the splitting as well as pull-out.
3) The proposed model, coupled 3D-RBSM and eight-noded solid FEM not only validates the experimental investigations effectively but also simultaneously captures the sensitivity analysis of friction. The numerical simulation results also highlight the importance and influence of test boundary conditions. It is evident from the numerical results, to obtain the deformation capacity and deformed behaviors accurately in the numerical simulations with high precisions, the test boundary conditions should be considered appropriately.

## REFERENCES

[1] Soroushian, P., Choi, K., Park, G. and Aslani, F., 1991. Bond of deformed bars to concrete: effects of confinement and strength of concrete. *ACI Materials Journal*. **88**:227-232.

[2] Kankam, C.K., 1997. Relationship of bond stress, steel stress, and slip in reinforced concrete. *J. Struct. Eng*. **123(1)**:79-85.

[3] Metelli, G. and Plizzari, G.A., 2014. Influence of the relative rib area on bond behaviour. *Institute of Civil Engineering*. **66(6)**:274-294.

[4] Xu, F., Wu, Z., Zheng, J., Hu, Y., and Li, Q., 2012. Experimental study on the bond behavior of reinforcing bars embedded in concrete subjected to lateral pressure. *Journal of Materials in Civil Engineering*. **24(1)**:125-133.

[5] Dawood, N. and Marzouk, H., 2012. Estimate of cracking and bond splitting stresses of reinforced concrete plates under uniaxial and biaxial tension. *ACI Structural Journal*. **109**:857-866.

[6] Chu, S.H. and Kwan, A.K.H., 2018. A new method for pull out test of reinforcing bars in plain and fiber reinforced concrete. *Engineering Structures*. **164**:82-91.

[7] Hayashi, D. and Nagai, K., 2013. Mesoscopic simulation of RC anchorage in multidirectional reinforcements by 3D discrete analysis. *J. JSCE*. **69**:241-257. [in Japanese].

[8] Hayashi, D., Nagai, K. and Eddy, L., 2017. Mesoscale analysis of RC anchorage performance in multidirectional reinforcement using a three-dimensional discrete model. *J. Struct. Eng*. **143(7)**:1-13.

[9] Matsumoto, K., Wang, T., Hayashi, D. and Nagai, K., 2016. Investigation on the pull-out behavior of deformed bars in cracked reinforced concrete. *Journal of Advanced Concrete Technology*. **14**:573-589.

[10] Eddy, L. and Nagai, K., 2016. Numerical simulation of beam-column knee joints with mechanical anchorages by 3D rigid body spring model. *Engineering Structures*. **126**:547-558.

[11] Eddy, L., Matsumoto, K. and Nagai, K., 2016. Effect of perpendicular beams on failure of beam-column knee joints with mechanical anchorages by 3D RBSM. *Journal of Asian Concrete Federation*. **2**:56-66.

[12] Kawai, T., 1978. New discrete models and their application to seismic response analysis of structures. *Nuclear Engineering and Design*. **48**:207-229.

[13] Yamamoto, Y., Nakamura, H., Kuroda, I. and Furuya, N., 2008. Analysis of compression failure of concrete by three-dimension rigid body spring model. *Doboku Gakkai Ronbunshuu*. **64(4)**:612-630. [In Japanese].

[14] Yamamoto, Y., Nakamura, H., Kuroda, I. and Furuya, N., 2014. Crack propagation analysis of reinforced concrete wall under cyclic loading using RBSM. *European Journal of Environmental and Civil Engineering*. **18**:780-792.

[15] Raymond, E., Untrauer. and Henry, R.L., 1965. Influence of normal pressure on bond strength. *Journal of the American Concrete Institute*. **62(5)**:577-586.

[16] Goto, Y., 1965. Cracks formed in concrete around deformed tension bars. *ACI Journal*. **68(4)**:244-251.

[17] Salem, H. M. and Maekawa, K., 2004. Pre- and post-yield finite element method simulations of bond of ribbed reinforcing bars. *J. Struct. Eng*. **4(671)**:671-680.